4. SITE 1045[1]

Shipboard Scientific Party[2]

HOLE 1045A

Position: 15°32.2407′N, 58°43.4222′W

Date occupied: 0200, 30 December 1996

Spud hole: 1445. 30 December 1996

End hole: 1945, 31 December 1996

Time on hole: 1 day, 17 hr, 45 min

Seafloor depth (drill-pipe measurement from rig floor, m): 4982

Distance between rig floor and sea level (m): 11.0

Water depth (drill-pipe measurement from sea level, m): 4971

Total depth (from rig floor, m): 5468

Penetration (m): 486

Total core recovered (m): 0

Comments: Logging while drilling (LWD). No coring done. Seafloor depth identified from LWD data

Principal results: Site 1045 was drilled through the décollement zone of the northern Barbados accretionary prism at 2.7 km west of the frontal thrust. This is the first penetration of a high-amplitude negative polarity reflection of the Barbados décollement zone. Previous modeling of the seismic data suggests that this reflection may indicate high fluid pressures and perhaps physical dilation and hydrofractures. Gamma ray, resistivity, density, caliper, photoelectric effect, and neutron porosity were logged (Fig. 3) to 58 m below the top of the décollement zone, where drilling stopped because of hole instability. Excluding neutron porosity, all logs are of excellent quality because of an in-gauge hole. Density measurements are reliable over 98% of the hole, where the differential caliper measurement is less than 1 in.

Traditional visual and multivariate statistical analyses of the logs define eight log units. Because Site 1045 was not cored, the lithology was inferred from log properties and seismic correlation with other sites. Carbonate-rich and clay-rich lithologies apparently dominate the accretionary prism, with a substantial clay-rich interval extending about 100 m above the décollement zone. Correlation of the logs with the seismic reflection data places an extremely low-density interval between 428 and 438 m below seafloor (mbsf) within the décollement zone. The density and resistivity curves correlate positively, except below the décollement zone. The density and resistivity trends are inverted along a thrust fault that can be identified in the seismic reflection data and also at several depths in the logs where no structures are resolved seismically.

The density log places significant constraints on the hydrogeology of the accretionary prism, décollement zone, and underthrust sediments. A reversal of the consolidation trend in density occurs about 100 m above the top of the décollement zone, near a thrust fault identified in the seismic data. The downward decrease in density toward the décollement zone suggests a pressure source within the décollement zone and a drain at the overlying thrust fault. Extremely low densities, down to 1.5 g/cm^3, characterize the décollement zone. Sharp changes in density (~0.2 g/cm^3) mark the top and bottom of the observed negative polarity reflection (Fig. 13). A comparison of the density profile through the proto-décollement zone at Site 1044 and the décollement zone at Site 1045 shows that the density lows at Site 1045 are slightly higher values, thinner, and more sharply defined than the broader low in the Site 1044 density data (Fig. 10). Therefore, the density distribution in the décollement zone can be explained by localized compaction of the proto-décollement zone, and dilation is not required. Beneath the décollement zone, consolidation in the clay-rich upper part of the underthrust section is retarded, probably by the same hydrologic conditions that retard the consolidation of the décollement zone.

BACKGROUND AND OBJECTIVES

Site 1045 is located about 2.7 km west of the frontal thrust of the accretionary prism and about 1.0 km west of Site 949 (Fig. 1). The seismic reflection data suggest that the décollement zone and oceanic crust are at about 425 and 800 mbsf, respectively (Fig. 2; also see Fig. 2 in the "Site 1044" chapter, back-pocket foldout, this volume). Several prominent thrust faults thicken the section in the accretionary prism at Site 1045.

The 3-D seismic reflection survey of the Leg 171A area indicates a large region of negative seismic polarity along the décollement zone beneath Site 1045 (Fig. 1B; Shipley et al., 1994; Moore et al., 1995). Seismic models of these negative polarity reflections predict that they are layers of low impedance (velocity × density) (Shipley et al., 1994; Bangs et al., 1996). Shipley et al. (1994) originally suggested that physical dilation produces the low impedance. Measurements of velocity, density, and effective stress of samples from the décollement zone and adjacent sediments support this interpretation (Tobin and Moore, 1997). Drilling at Site 947 during Leg 156 was an attempt to test the hypothesis that dilation causes the negative polarity reflections. However, penetration at Site 947 stopped 60 m above the décollement zone because of hole instability, probably resulting from high fluid pressure (Shipboard Scientific Party, 1995a).

LWD at Site 1045 was intended to establish the physical properties of the negative polarity reflection of the décollement zone. The negative polarity reflection beneath Site 1045 is part of the seaward portion of a regional northeasterly trending band of negative polarity reflections that underlies the accretionary prism (Fig. 1B). The negative polarity reflection at Site 1045 occurs at a significantly shallower depth than the similar reflection at Site 947. Because the décollement zone is at a shallower depth, the difference between the potentially lithostatic fluid pressure in the décollement zone and the hydrostatic fluid pressure in the borehole is correspondingly less, and the chance of hole problems is diminished. The amplitude of the negative polarity reflection decreases sharply seaward toward Site 949, where the décollement zone reflection is indistinct.

Another major goal of Site 1045 was to determine the consolidation of the underthrust section caused by burial by the overlying accretionary prism. Water produced by the consolidation of the underthrust section is a significant driving force in the hydrologic system

[1]Moore, J.C., Klaus, A., et al., 1998. *Proc. ODP, Init. Repts.*, 171A: College Station, TX (Ocean Drilling Program).

[2]Shipboard Scientific Party is given in the list preceding the Table of Contents.

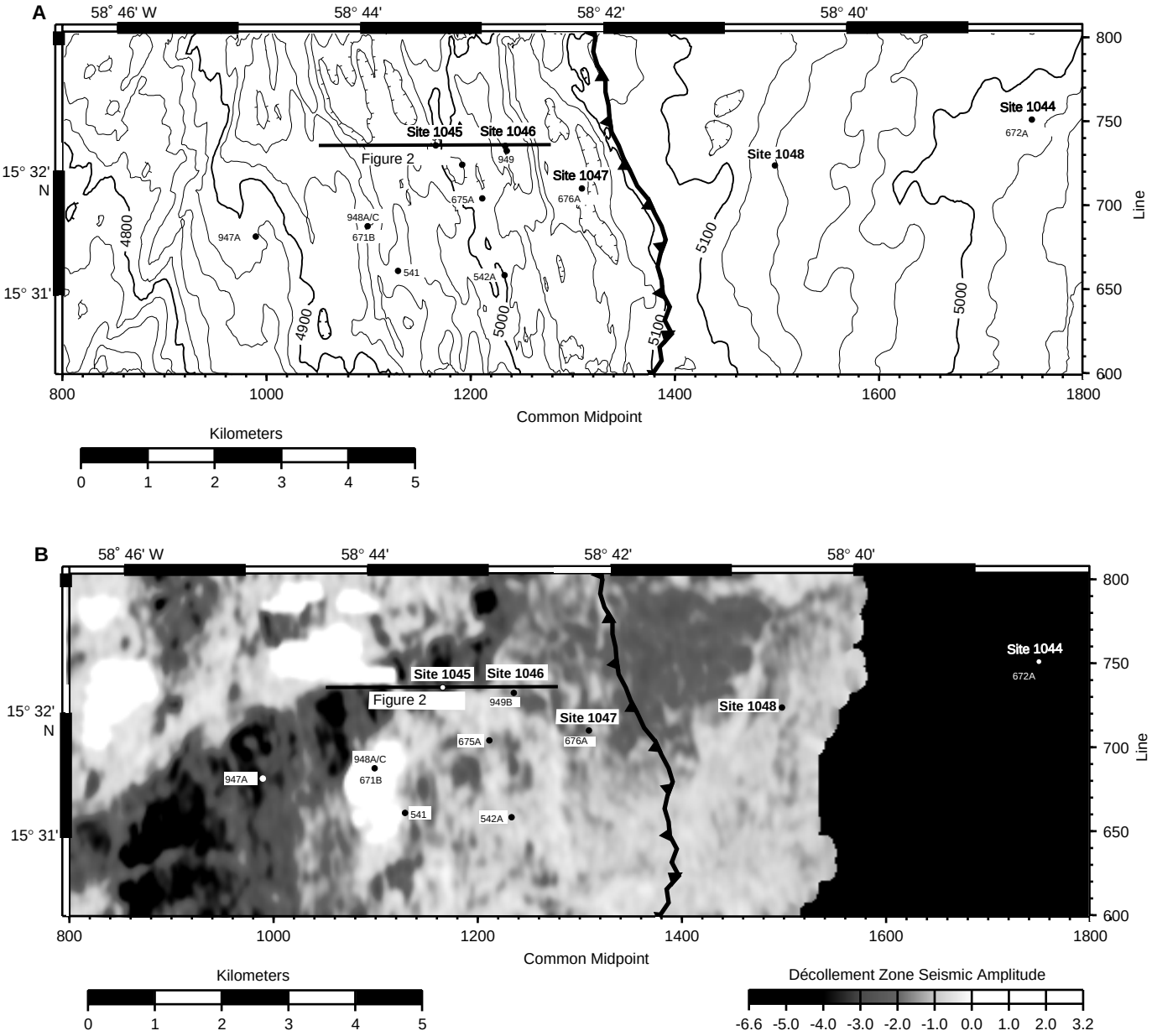

Figure 1. **A.** Bathymetic location map for Site 1045 in the Leg 171A drilling area and for previous ODP and Deep Sea Drilling Project holes in the northern Barbados accretionary prism. **B.** Map of peak seismic amplitude of the décollement reflector of the northern Barbados accretionary prism in the Leg 171A drilling area.

of the accretionary prism (Screaton et al., 1990; Bekins et al., 1995). Comparison of log-derived lithologic and porosity data from Sites 1044 and 1045 will determine the amount of water flux from the underthrust sediments.

Site 1045 was not cored and therefore has a paucity of comparative information. Nevertheless, correlations from nearby sites through the 3-D seismic data with the inherent nature of the logs should provide basic lithologic information.

OPERATIONS

Hole 1045A

The vessel was offset in dynamic positioning mode at a speed of 2 nmi/hr from Hole 1044A to Site 1045, while retrieving the bottom-hole assembly (BHA) and downloading the LWD data from Hole 1044A. The distance between Sites 1045 and 1046 is ~1 km, and one beacon was dropped between these sites and used for operations at both locations. LWD Hole 1045A was located at Global Positioning System (GPS) coordinates 15°32.2407′N, 58°43.4222′W. After changing out the LWD tools, the same BHA from Hole 1044A was assembled with a new Smith $9^{7}/_{8}$-in FDGH (3 × 14) bit. Hole 1045A was spudded at 1445 hr on 30 December 1996. Drilling was initiated at a water depth of 4980.4 m below rig floor (mbrf) based on the precision depth recorder (PDR) reading. As at all the LWD sites, it was not possible to determine the mudline in the soft sediments with the drill pipe. Therefore, the PDR reading of 4980.4 mbrf was used for the initial water depth. The actual water depth was established at 4982 mbrf (4971 m below sea level [mbsl]) based on analysis of the LWD data.

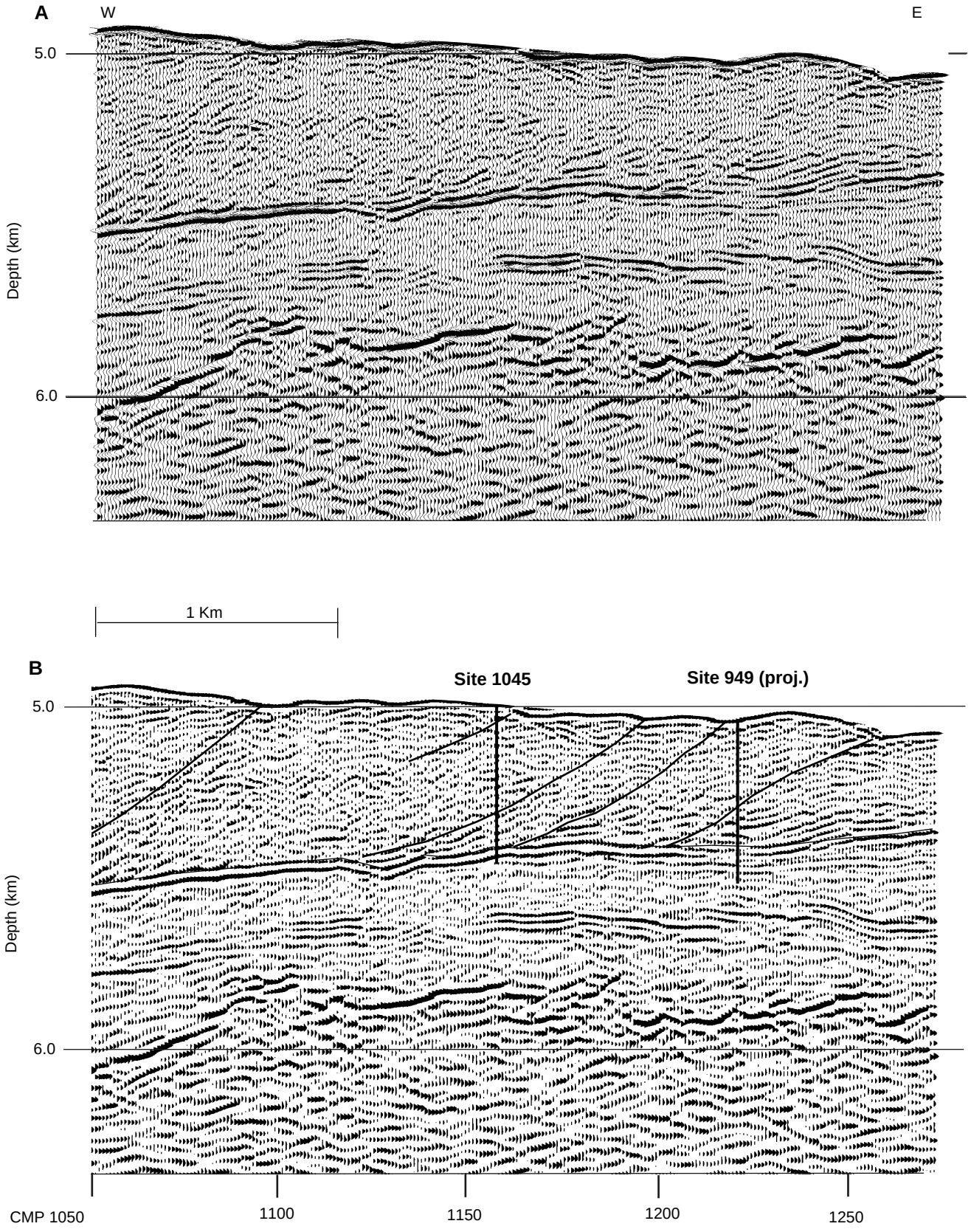

Figure 2. (**A**) Uninterpreted and (**B**) interpreted seismic Line 739 through Site 1045 (see Fig. 1 for location). Black is positive polarity; white is negative polarity. Site 949 is projected from the south. The amplitude of the negative polarity reflection decreases from beneath Site 1045 to Site 949.

We attempted to drill at 35 m/hr down to 5416 mbrf (434 mbsf), where high pump pressure and torque were encountered. The décollement zone was estimated to be at 424 mbsf, and considerable back reaming and hole conditioning were required to advance the drill string beyond this point. The drill string was pulled up to 5371 mbrf (389 mbsf), and a 30-barrel sepiolite mud sweep was pumped. The hole was then reamed back down from 5371 to 5416 mbrf (389 to 434 mbsf, respectively). Drilling continued to 5468 mbrf (486 mbsf), where the hole packed off and high pump pressures and torque occurred. Rotation and 30,000 lb of overpull were required to pull the drill string back up the hole.

A request was made to the Ocean Drilling Program (ODP) for permission to deepen Site 1046 by 250 m, from 600 to 850 mbsf, to achieve the deeper depth objectives below the décollement zone (underthrust section) that we suspected could not be achieved in Hole 1045A. ODP granted permission for an additional 250 m (±25 m) penetration or first contact with basement at Site 1046. Because the total time on the LWD tool batteries was approaching 48 hr, with a maximum of 100 hr, the decision was made to abandon Hole 1045A and to offset in dynamic positioning mode to Site 1046. The remaining battery time would be sufficient for drilling Hole 1046A without having to trip the drill string, resulting in a time savings of ~20 hr. The drill string was pulled out of the hole and the seafloor was cleared at 1945 hr on 31 December to end Hole 1045A. The drill string was pulled an additional 50 m above the seafloor, and the vessel was offset in dynamic positioning mode to Site 1046.

CHARACTERIZATION OF LOGS

Definition of Log Units

The log data, with the log units labeled, are shown in Figure 3. We defined six log units and several subunits through a combination of visual interpretation and multivariate statistical analysis (Fig. 4; see "Explanatory Notes" chapter, this volume).

Three factors were extracted from the deep resistivity, gamma-ray, thorium, potassium, photoelectric effect, and bulk density logs. Because of a large scatter in the neutron porosity data, they were not used. Excluding these neutron porosity data reduced the variance in the data, as explained by the factor logs from 90% to 86%. The three factor logs explain 90% of the variance contained in the data, and the cluster analysis shows five prominent clusters. In Table 1, the mean values and standard deviations of the log properties are summarized by cluster, each of which shows a distinct set of physical properties. The calculated cluster log is shown together with the log units and the gamma ray and density in Figure 4.

The base of log Unit 1 (0–48.1 mbsf) is defined by a 0.2-Ωm decrease in resistivity that coincides with a decrease in the bulk density of 0.2 g/cm^3 and a gradual decrease in photoelectric effect.

The base of log Unit 2 (48.1–76.6 mbsf) has a 0.2-Ωm increase in resistivity, a 1.0-barns/e$^-$ increase in photoelectric effect, and a 0.1-g/cm^3 increase in density.

Log Unit 3 (76.6–164.7 mbsf) is generally characterized by a gradual increase in resistivity and density from 0.9 to 1.2 Ωm and from 1.6 to 1.9 g/cm^3, respectively. Subunit 3a (76.6–117.3 mbsf) has a high (0.06) neutron porosity standard deviation that decreases to 0.57 at the Subunit 3a/3b boundary. The base of Subunit 3b (117.3–164.7 mbsf) has negative shifts in density, photoelectric effect, deep resistivity, and shallow resistivity of 0.2 g/cm^3, 1.0 barns/e$^-$, 0.4 Ωm, and 0.5 Ωm, respectively.

The base of log Unit 4 (164.7–182.2 mbsf) is the midpoint of a gradual change from 0.57 to 1.2 Ωm in the shallow resistivity over a 9-m interval.

The base of log Unit 5 (182.2–318.0 mbsf) is defined by a change in the character of the resistivity, photoelectric effect, density, and gamma-ray logs. Log Unit 5 is dominated by cluster 4 (Fig. 4; Table 1), which has a high standard deviation in resistivity (0.09 Ωm). The gamma ray is also variable (with a fairly high standard deviation of 9.7 GAPI), but slowly decreases from 95 GAPI at the top to 70 GAPI at 300 mbsf, then increases again to about 120 GAPI at the base of Unit 5, where it starts to decrease. The density increases through Unit 5 from 1.7 to 2.0 g/cm^3, and then decreases in Unit 6. The photoelectric effect remains fairly consistent (standard deviation of about 0.3 barns/e$^-$) through log Unit 5, and then starts a gradual decrease at the Unit 5/6 boundary.

Unit 6 (318.0–424.9 mbsf) is characterized by gradual decreases in bulk density, photoelectric effect, gamma ray, and resistivity from 2.0 to 1.75 g/cm^3, 4.0 to 1.5 barns/e$^-$, 120 to 50 GAPI, and 1.15 to 0.7 Ωm, respectively. The variability of the neutron porosity, photoelectric effect, and bulk density increases within Unit 6 between 410 and 425 mbsf (just above the décollement zone). The base of Subunit 6a (318.0–360.0 mbsf) is the midpoint of a zone between 350 and 370 mbsf, where the cluster analysis shows a gradual change in character (Fig. 4). The Subunit 6a/6b boundary is not well defined compared with other boundaries, because there are no obvious shifts in any of the logs. The base of Subunit 6b (360.0–424.9 mbsf) has a negative shift in the bulk density of 0.3 g/cm^3, a 0.25-Ωm shift in the resistivity logs, and a minimum gamma-ray value of 50 GAPI.

The base of log Unit 7 (424.9–438.1 mbsf), is defined by a decrease in standard deviation of neutron porosity and photoelectric effect, an increase in resistivity of 0.15 Ωm, and an increase in bulk density of 0.2 g/cm^3. The Unit 7/8 boundary is also the midpoint of a gradual increase in the gamma ray.

Log Unit 8 is characterized by increasing density, gamma ray, and resistivity, and by a lower standard deviation (0.67 in Unit 7, 0.6 in Unit 8) in neutron porosity.

LWD Log Quality

For Hole 1045A, a target rate of penetration (ROP) of 35 m/hr was chosen because we concluded that in Hole 1044A, the gamma-ray data collected by the natural gamma-ray tool (NGT) at 30- to 40-m/hr penetration rates are reliable (see "Characterization of Logs" section, "Site 1044" chapter, this volume). A ROP of ~35 m/hr was maintained throughout Hole 1045A (Fig. 5).

The differential caliper values in Hole 1045A show standoffs of less than 1 in, except for a few small intervals at 0–20 mbsf, 435 mbsf (1.01 in), and 437 mbsf (1.07 in).

Zones of minor washout are identified in intervals 0–20, 45–78, 165–190, 247–267, and 410–438 mbsf. Overall, borehole conditions were excellent; 97.6% of the hole showed a differential caliper of <1 in, and 91.2% showed values <0.5 in. The bulk density correction (DRHO) varies from –0.07 to 0.07 g/cm^3, which indicates that high-quality density measurements were obtained. Time-after-bit (TAB) measurements are 10 to 40 min for resistivity and gamma-ray measurements and 30 to 80 min for density and neutron porosity measurements. High TAB values, up to 200 min, in the interval from 433 to 444 mbsf coincide with a wiper trip. A part of the wiper trip interval coincides with the minor washout interval at 410–438 mbsf; however, the differential caliper and DRHO logs indicate that the borehole conditions did not deteriorate significantly during the wiper trip, (i.e., between the time of drilling and the time of measurement).

LOGS AND LITHOLOGY

Site 1045 is not located adjacent to a previously cored hole. Thus, we interpret the lithology from the log response and reference to nearby sites cored during Legs 110 and 156 (Fig. 6).

Site 1045

Log Unit 1 (0–48.1 mbsf)

Within LWD log Unit 1, the gamma-ray log decreases to a low at 12 mbsf and increases to the bottom of the unit, whereas the photoelectric effect increases throughout the unit. The responses are con-

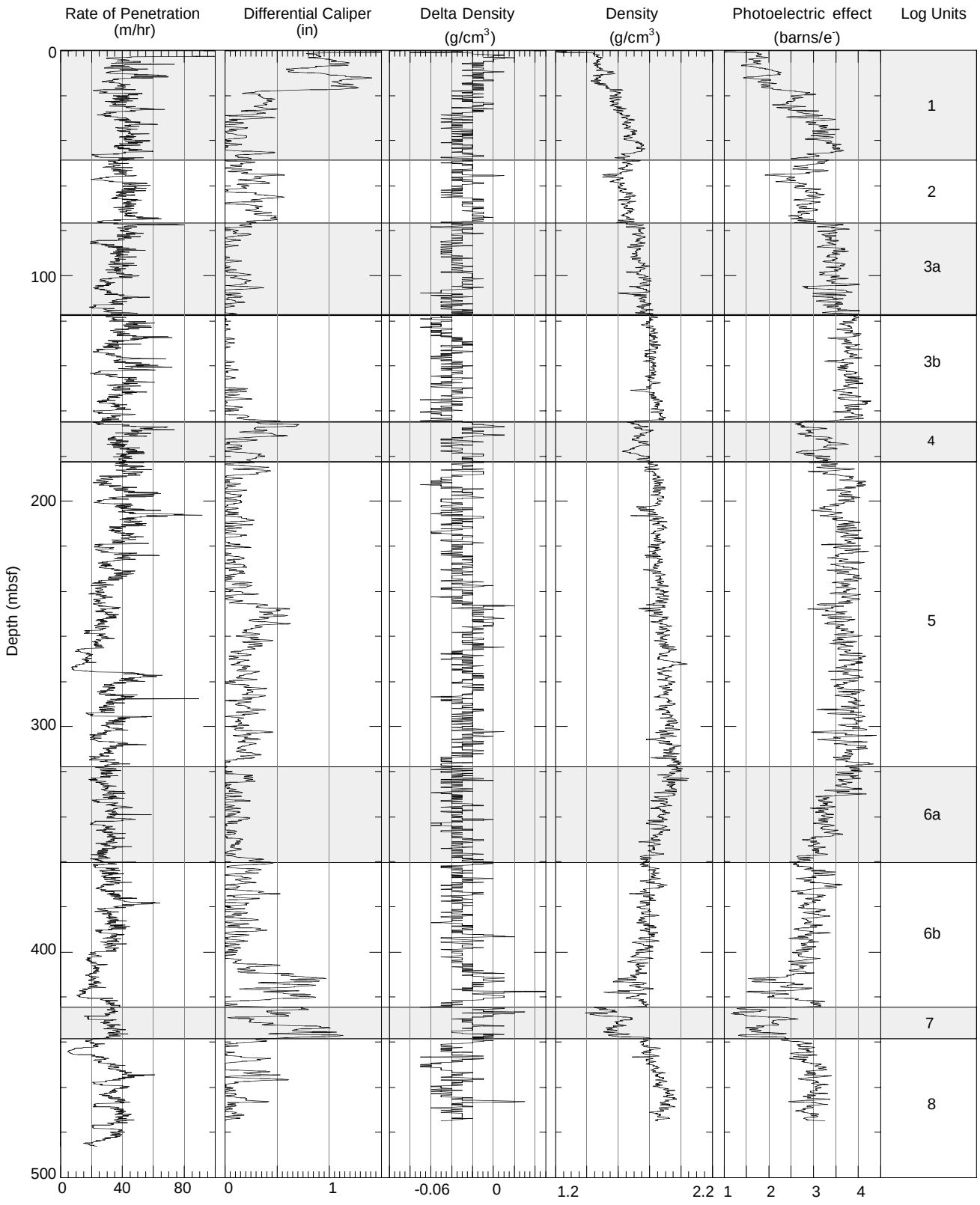

Figure 3. Site 1045 LWD data and log units. Post-cruise processed log data are available on CD-ROM (back pocket, this volume).

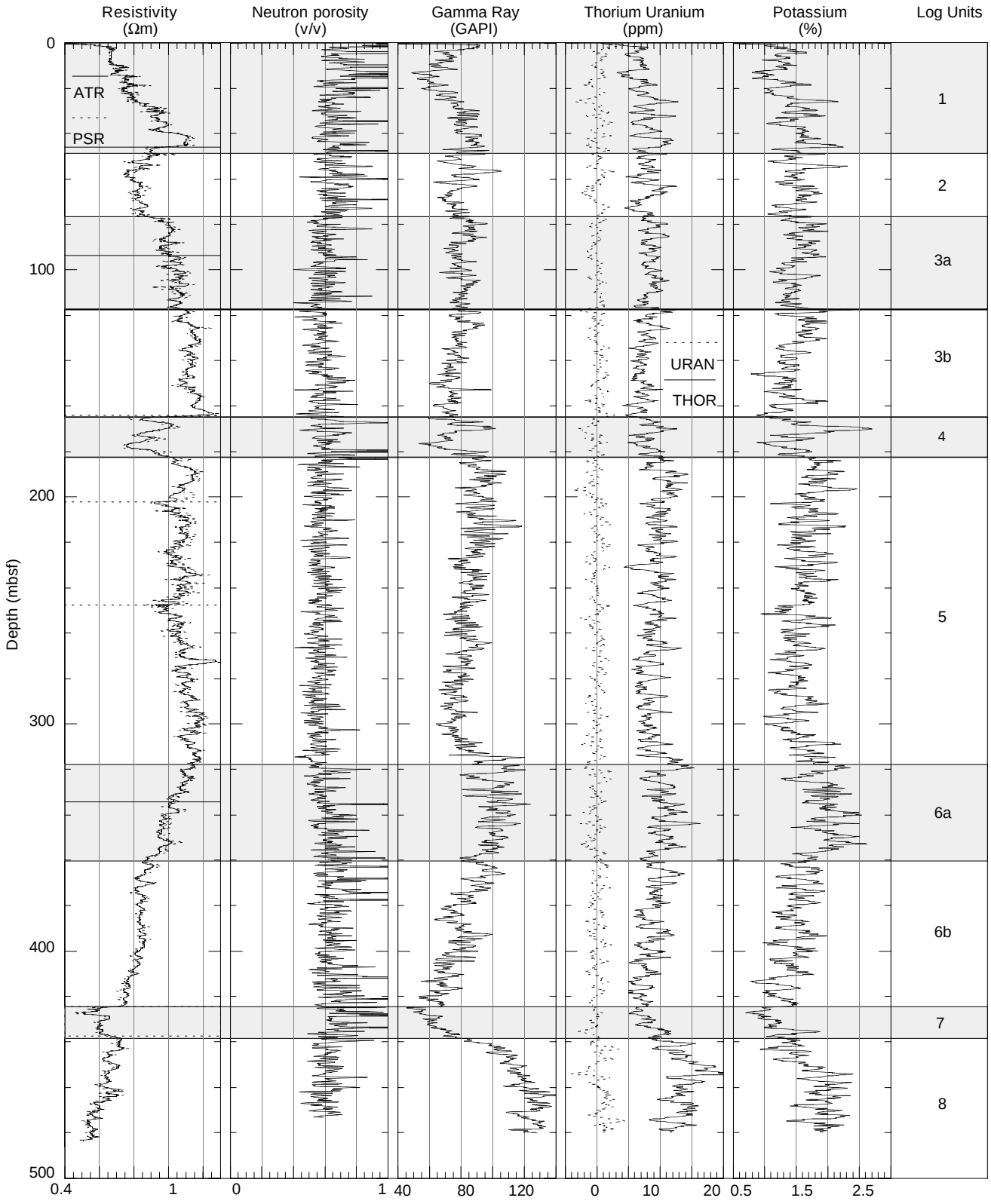

Figure 3 (continued).

Table 1. Mean values and standard deviations of the log properties according to each cluster for Hole 1045A.

	ATR (Ωm)		GR (GAPI)		THOR (ppm)		POTA (%)		PEF		ROMT (g/cm^3)	
	Mean	SD	Mean	SD	Mean	SD	Mean	SD	Mean	SD	Mean	SD
All	0.96	0.16	85.13	14.61	9.13	2.36	1.58	0.31	3.29	0.54	1.80	0.10
Cluster 1	0.77	0.10	71.10	10.16	7.61	1.55	1.34	0.28	2.43	0.45	1.63	0.06
Cluster 2	0.94	0.10	81.68	7.65	8.60	1.47	1.57	0.27	3.17	0.31	1.75	0.05
Cluster 3	1.12	0.05	77.10	5.66	7.52	1.20	1.46	0.24	3.81	0.17	1.86	0.05
Cluster 4	1.05	0.09	94.85	9.68	10.52	1.58	1.76	0.28	3.60	0.33	1.88	0.05
Cluster 5	0.65	0.05	117.08	10.50	14.21	2.13	1.80	0.29	2.95	0.18	1.85	0.05

Notes: SD = standard deviation; ATR = attenuation resistivity; GR = gamma ray; THOR = thorium; POTA = potassium; PEF = photoelectric effect; ROMT = density (rotationally processed).

sistent with the overall increase in calcareous material found in the lower Pleistocene to upper Miocene units at Sites 672 and 948.

Log Unit 2 (48.1–76.6 mbsf)

A reduction in photoelectric effect and density accompanied by a decrease in resistivity over log Unit 2 is associated with faulting rather than a change in lithology.

Log Unit 3 (76.6–164.7 mbsf)

A steadily increasing photoelectric effect and increasing density and resistivity suggest a normal compaction profile of the calcareous sediments within log Unit 3. Local high spikes in potassium (120 and 170 mbsf) could be caused by ash layers in the Pleistocene to Pliocene units at Sites 672 and 671 (Wang et al., 1990).

Log Unit 4 (164.7–182.2 mbsf)

A reduction in resistivity, photoelectric effect, and density in log Unit 4 appears to correspond to a possible fault imaged by the seismic data. There is no evidence that the lithology changes significantly across the fault.

Log Unit 5 (182.2–318 mbsf)

The characteristically high photoelectric effect, density, and resistivity and low gamma ray may be associated with carbonate in Unit 5. The data suggest that the calcareous lithology present to a depth of 360 mbsf at Site 671 is also probably present at this site to a depth of 318 mbsf.

Log Unit 6 (318–424.9 mbsf)

Log Unit 6 is the deepest stratigraphic unit overlying the décollement zone. A large fault at 334 mbsf is clearly imaged in the seismic data. At approximately this depth, there is an abrupt increase in gamma ray (315 mbsf) and a decrease in photoelectric effect (330 mbsf). These changes are consistent with a change in lithology to carbonate-poor clays below the fault. Below this depth, decreases in resistivity, potassium, gamma ray, photoelectric effect, and density are consistent with an increase in porosity with depth within log Unit 6. A lithologic change from calcareous to siliceous sediments would cause the same reduction in the photoelectric effect without any reduction in either gamma ray or density, as is seen in this section. If the carbonate material had been replaced by more clay-rich sediments, the gamma ray would be expected to increase; however, this is not the case. Instead, the gamma ray decreases, which usually indicates a decrease in clay content. As few of the lithologic indicators imply a change in lithology, the log responses are interpreted as being caused by a change in porosity.

Log Unit 7 (424.9–438.1 mbsf)

Log Unit 7 has large differential caliper readings and the resistivity and photoelectric effect logs show low values. However, the interval from 400 to 424.9 mbsf has the same large caliper readings but much higher density and resistivity readings, indicating that the large caliper readings are unlikely to be the cause of the low log readings in log Unit 7. This suggests high porosity within the unit. The underconsolidated décollement zone at Site 1045 is interpreted to include this unit.

Log Unit 8 (438.1–473.2 mbsf)

There is a large increase in gamma ray at 438 mbsf, and the thorium/potassium ratio increases from 6 to 12. This high ratio suggests the presence of smectite, which is consistent with the clay mineralogy at this stratigraphic level at Sites 671 and 672 (Tribble, 1990). Clay mineralogies at Sites 948 and 949, however, indicate an increase in illite and a decrease in smectite at this level (Underwood and Deng, 1997). This log unit is characterized by low resistivity and photoelectric effect, high gamma ray, and higher density than the previous units. It is inferred that a clay-rich, low-carbonate section was penetrated.

Summary

The carbonate-rich interval penetrated at Sites 672 and 949 is probably also present at Site 1045, where the carbonate content appears to decrease downward sharply across a major fault at 334 mbsf.

1. A package of horizontal, parallel reflectors above the décollement zone is inferred to be low-carbonate clays at Site 1045, as at Sites 1044 and 1046.
2. A downward decrease in density in log Unit 6 is caused by underconsolidation rather than lithology.

LOGS AND STRUCTURE

Hole 1045A penetrates two thrust faults and the décollement zone, which are identified in seismic reflection Line 739 (Fig. 2). A fault at 46 mbsf is defined by a bathymetric offset on the seafloor, suggesting thrust displacement. The second fault, at 334 mbsf, is marked by a clear transition on the seismic line from approximately horizontal beds in the hanging wall to gently dipping beds in the footwall. Figure 7 shows the position of these faults relative to the LWD logs. The uppermost thrust fault coincides with the boundary between log Units 1 and 2. The density inversion that marks this boundary is consistent with thrust faulting. The second thrust fault is 16 m below the boundary between log Units 5 and 6. There may be some miscorrelation between the seismic and LWD depths, and the rever-

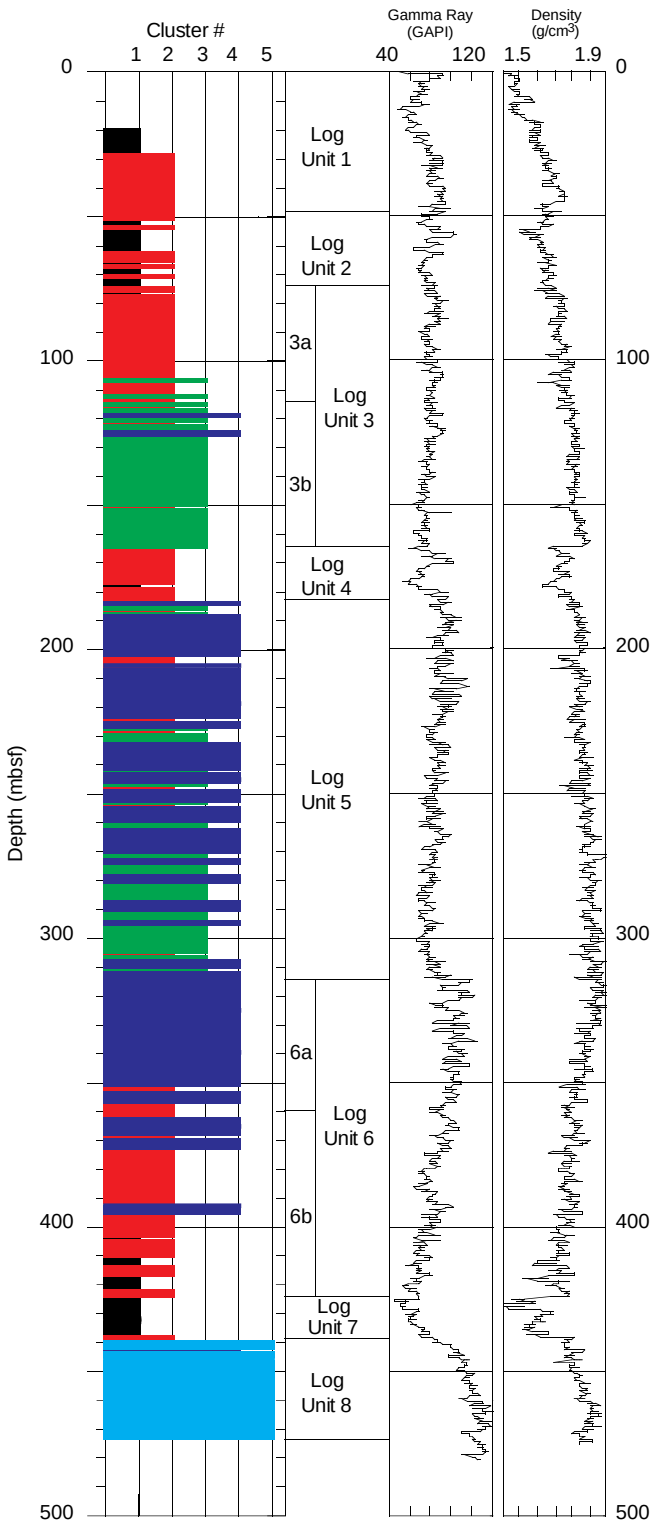

Figure 4. Definition of log units for Site 1045. Five clusters were derived from three factor logs that account for 90% of the total variance observed in the data (Table 1). Boundaries between first-order log units correspond to changes in log character that are related primarily to lithology and that are clearly visible on the logs (e.g., gamma ray, density, photoelectric effect, and resistivity). Second-order units represent subtle changes in log character that are observed in only a few curves and that may not be related to lithology.

sal in trend of both density and resistivity at the boundary between log Units 5 and 6 may be related to this thrust. The décollement zone reflector correlates well with the boundary between log Units 6 and 7.

Three additional possible faults are indicated by LWD data that show inversions in density and resistivity as well as changes in the photoelectric effect and caliper measurement (Fig. 7). Seismic data do not confirm the presence of these faults, perhaps because of the coarseness of the resolution. However, discontinuous, erratic reflections throughout the prism suggest the presence of numerous, smaller scale faults that cannot be clearly identified in seismic data (Fig. 2). The small changes in log character suggest the presence of small displacement faults that are consistent with the general character of the prism.

LOGS AND PHYSICAL PROPERTIES

This section covers the results of LWD that are indicative of the sediment bulk physical properties. In particular, downhole trends in the rotationally processed density, photoelectric effect, and resistivity logs are described. The density log is discussed in terms of its relation to sediment consolidation and deformation above and below the décollement zone. As there are no core-derived physical properties data, we lack the grain density information necessary to calculate a reliable porosity profile. However, we present computed porosities based on resistivity information and compare them with a porosity profile based on a constant grain density. Of particular importance to the overall goals of this site is a comparison of the density profile of the underthrust section with that of the reference section, as it can help identify the amount of fluid available for expulsion from the underthrust section.

Density

The downhole density profile is characterized by several intervals that display well-defined trends with depth. They correspond to the major log units, and their boundaries can be correlated with structural features seen in the seismic section and with lithologic changes in the reference section at Site 1044 (Table 2; Fig. 8).

The uppermost part of the section is characterized by a constant increase in density between 0 and 44 mbsf, with a mean density of 1.58 g/cm^3. The top 20 m is probably affected by washouts, as indicated by differential caliper readings greater than 1 in. The abrupt drop in density at 44 mbsf is clearly related to the penetration of a shallow thrust just above the log unit boundary (seen in seismic sections).

The interval between 48 and 77 mbsf shows a sharp rise in density. The average density over the whole interval is 1.64 g/cm^3. The interval from 77 to 162 mbsf shows steadily increasing density with depth, which agrees with a normal consolidation trend. The average density is 1.78 g/cm^3. The lower boundary of this interval is marked by a sharp fall in density from 1.9 to 1.65 g/cm^3, coincident with the penetration of another thrust fault at this depth (also see “Logs and Structure” section, this chapter). Over an interval of 15 m (162–177 mbsf), densities show a lower average value of 1.73 g/cm^3, followed by another shift to higher values at the lower boundary.

From 177 to 318 mbsf, density values show a steady increase that is, again, consistent with normal consolidation. Over the interval from 318 to 425 mbsf, density values steadily decrease with depth from about 1.95 g/cm^3 at 320 mbsf to about 1.7 g/cm^3 at 420 mbsf, with an overall average of 1.81 g/cm^3 (Table 2). This anomalous downhole trend may be related to another seismically identified prominent thrust fault at the top of the interval, which could inhibit the dewatering of the sequence. Alternatively, the observed pattern could be caused by the sequence itself having low permeability and

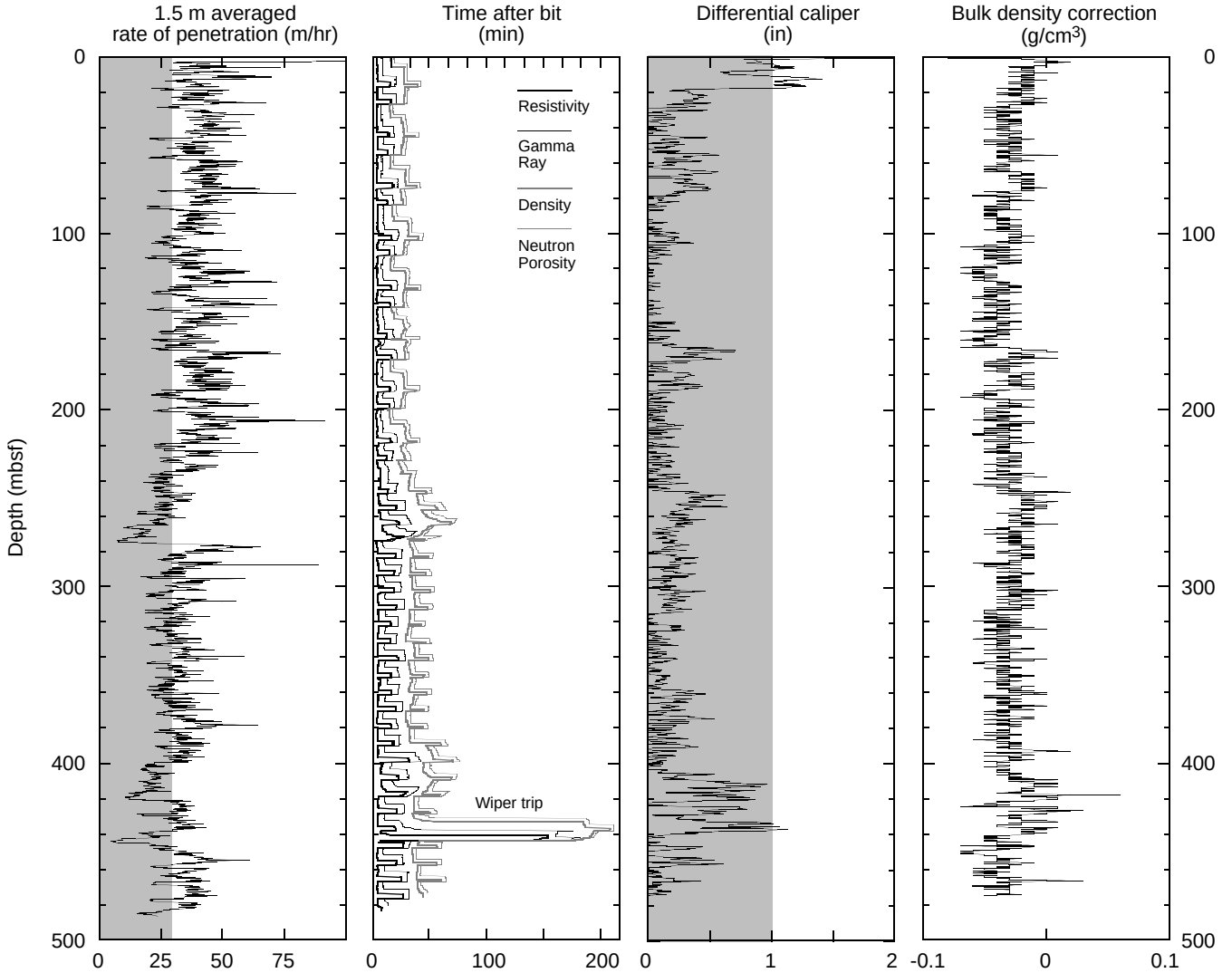

Figure 5. Summary of the quality-control logs. The shaded area in the ROP shows the reliable zone for NGT measurements according to industry experience. The shaded area in the differential caliper indicates good borehole conditions.

being slow to dewater, or by high pore pressure associated with the décollement zone.

The interval from 429 to 439 mbsf, the depth of the negative-polarity seismic reflector, is marked by another significant offset toward lower densities. Minima are as low as 1.4 g/cm³. The average density of the sediments within the décollement zone is 1.57 g/cm³. The differential caliper log indicates a higher degree of borehole washout over most of the décollement zone (Fig. 9), with peak values slightly in excess of 1 in. However, this does not seem to greatly alter the observed general density pattern in the décollement zone.

The top 48 m of the underthrust sequence penetrated below the décollement zone (439–487 mbsf) is characterized by a clear offset toward higher densities, with a subsequent downhole density increase. The average density in the interval between 439 and 487 mbsf is 1.85 g/cm³. The small-scale variations seem to match those observed in the stratigraphically equivalent section in the reference section (Fig. 10).

Photoelectric Effect

As seen in Hole 1044A, the characteristics of the photoelectric effect downhole profile closely match the trends observed in the density log (Fig. 11). The divisions defined for the density and resistivity logs can also be applied to the photoelectric effect log. Changes in character at 117 and 360 mbsf, which correspond to the subdivision boundaries within log Units 3 and 6, are not seen in the bulk density log.

Resistivity Logs

The deep and shallow resistivity logs are almost identical in character, although the deep resistivity has a lower resolution (Fig. 8B). The broad resistivity trend entails a gradual increase from 0 to 130 mbsf, followed by constant values (1.0–1.1 Ωm) to 310 mbsf. The resistivity then gradually decreases from 310 mbsf to the bottom of the hole at 480 mbsf, where the resistivity values are about 0.55 Ωm. Three zones have lower resistivity values than the overall trend: 48.1–76.6 mbsf (log Unit 2), 164.7–182.2 mbsf (log Unit 4), and 424.9–438.1 mbsf (log Unit 7).

Density and Resistivity Porosity

The density porosity was calculated from a seawater density of 1.02 g/cm³ and a grain density of 2.655 g/cm³. The grain density is

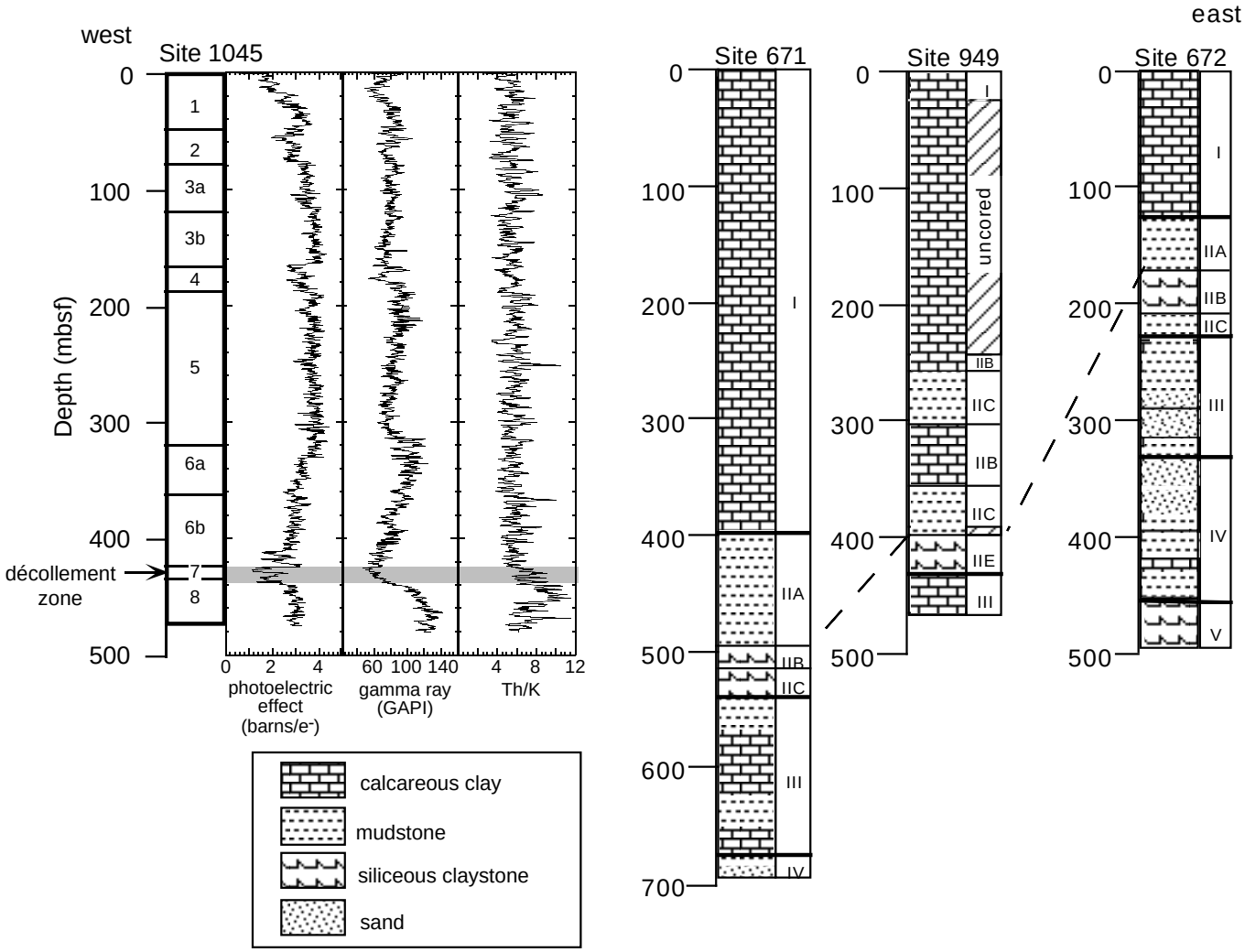

Figure 6. Summary of Site 1045 log units correlated with lithologic units defined at nearby Sites 949 and 671 and reference Site 672 (see "Logs and Lithology" section, "Site 1044" chapter, this volume, for detailed information about log units for Site 1044). Sites are depicted along a west to east transect. The lithology above the décollement zone (tops connected with dashed line) is similar at all three cored sites, with calcareous claystones and marls overlying noncalcareous clays. The broad peak in the thorium/potassium ratio is consistent with the presence of a smectite-rich layer that underlies the siliceous clays of the décollement zone at Sites 671 and 672. See text for further discussion. Figure adapted from Shipboard Scientific Party (1988b, 1995b).

the median grain density measured at Site 949 (Shipboard Scientific Party, 1995b), the closest cored site to Site 1045. The resistivity porosity was calculated using the Archie coefficients a = 0.988 and m = 2.352. These coefficients were estimated using formation factor and density porosity data only from above the décollement zone (see "Explanatory Notes" chapter [this volume] for details).

A comparison of the density and resistivity porosities (Fig. 12) demonstrates good correlation above 340 mbsf. The resistivity porosity is 2% to 4% higher than the density porosity in the interval at 0–180 mbsf, but the porosity curves are almost identical from 180 to 340 mbsf. Between 340 and 400 mbsf, the resistivity porosity is 0% to 9% lower than the density porosity. Below the décollement zone (439–487 mbsf), the resistivity porosity is 0% to 10% higher than the density porosity.

The character of the density and resistivity logs is reflected in the respective porosity logs. The resistivity porosity shows less variability than the density porosity. The high variability of the density log (possibly resulting from hole size variation; see the differential caliper in Fig. 3) and consequently creates a highly variable density porosity log. In contrast, the resistivity porosity is less sensitive to hole size variation. However, because the resistivity porosity is calculated from Archie's law, which was intended for sandy formations (as opposed to formations with a high amount of conductive clay), the validity of the resistivity porosity log is questionable (see "Explanatory Notes" chapter, this volume).

Comparison With Site 1044

To examine the change in physical properties as sediments are loaded by accretion, density and resistivity logs from the décollement zone and underthrust sediments at Site 1045 are compared with those from the proto-décollement zone and underthrust sediments at Site 1044 (Fig. 10). The depths were shifted by visually correlating distinctive variations on the resistivity logs. The depth scales are the same for both sites. The proto-décollement zone at Site 1044 appears as a broad interval of low density, whereas the (inferred) décollement zone appears at Site 1045 as three or four low-density spikes separated by higher density material. The lowest density at Site 1045 is 1.39

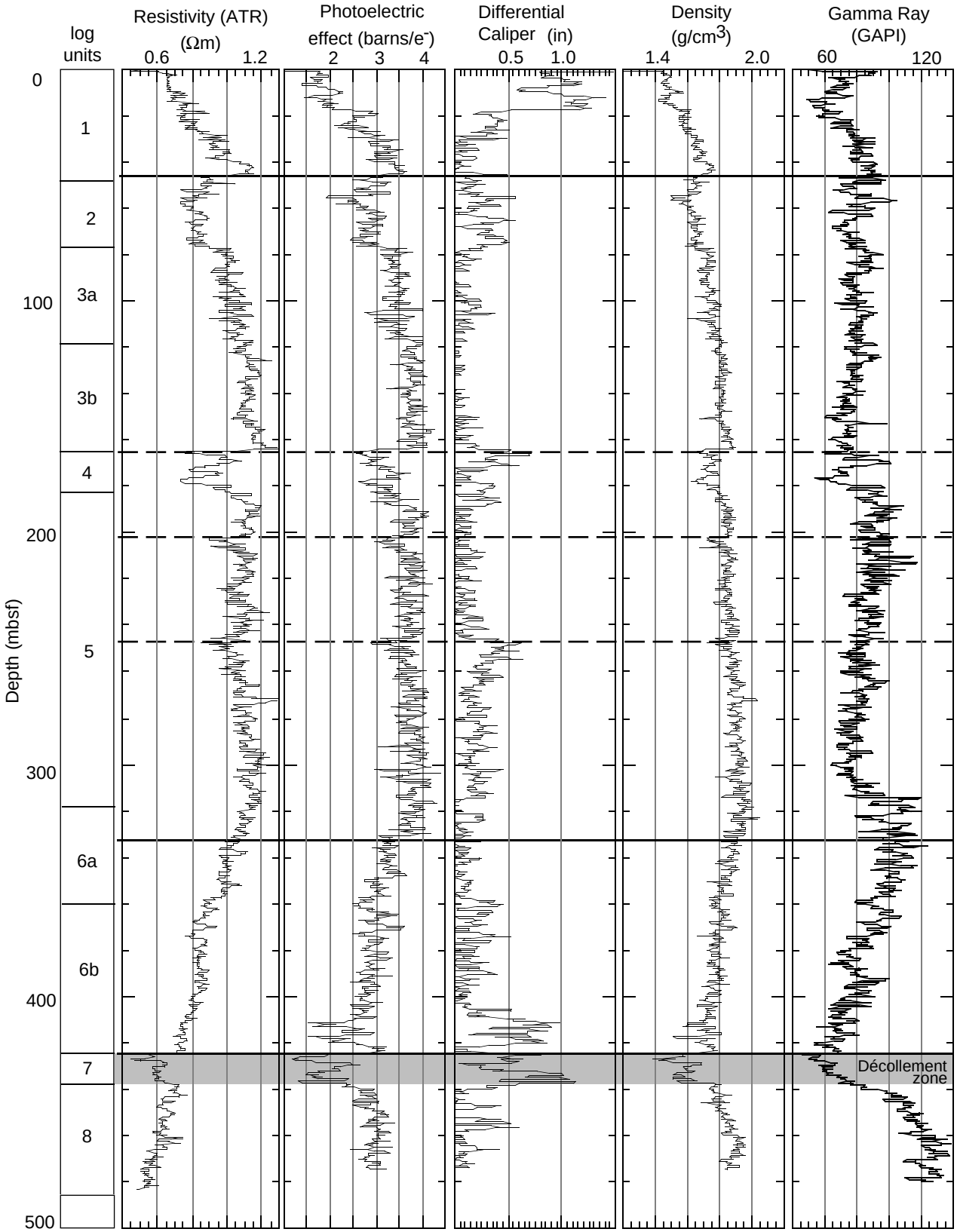

Figure 7. Structural interpretation of Hole 1045A LWD data. Lines show positions of faults imaged in the seismic data. Dashed lines indicate faults interpreted from decreases in density, resistivity, and photoelectric effect, and increases in differential caliper.

Table 2. Density profile division with mean values and standard deviations.

Depth (mbsf)	Mean density (g/cm^3)	Standard deviation (g/cm^3)	Characteristics	Tentative interpretation
0-44	1.58	0.11	Rapid rise with depth	Normal consolidation trend, affected by high ROP
44-77	1.64	0.04	Sharp fall, then rise	Inversion - thrust fault
77-162	1.78	0.06	Steady rise with depth	Normal consolidation trend
162-177	1.73	0.04	Sharp drop, then increase	Inversion - thrust fault
177-318	1.87	0.05	Steady increase with depth	Normal consolidation trend
318-424	1.81	0.08	Rapid steady decrease with depth	Underconsolidated - increase in porosity with depth
424-439	1.57	0.07	Sharp fall to steady low value	Décollement zone
439-487	1.85	0.06	Sharp rise to peak	Underthrust sequence - normal consolidation trend

Note: ROP = rate of penetration.

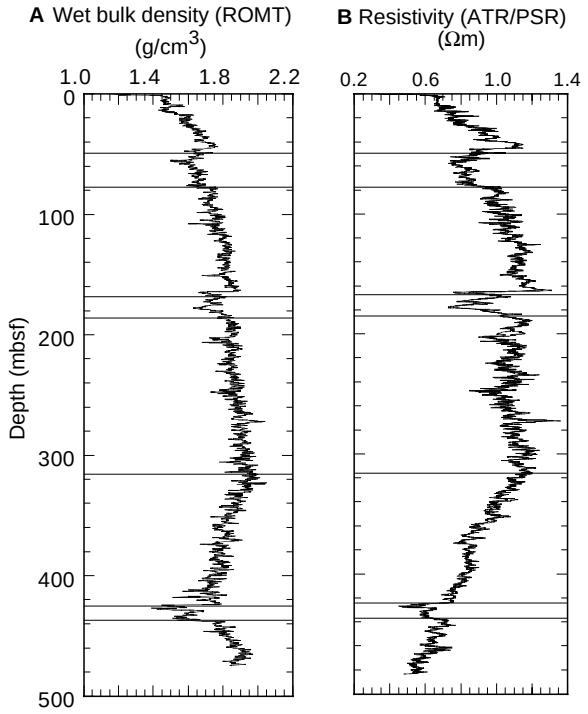

Figure 8. (**A**) Density and (**B**) resistivity vs. depth in Hole 1045A. Lines separate intervals discussed in the text (major log units).

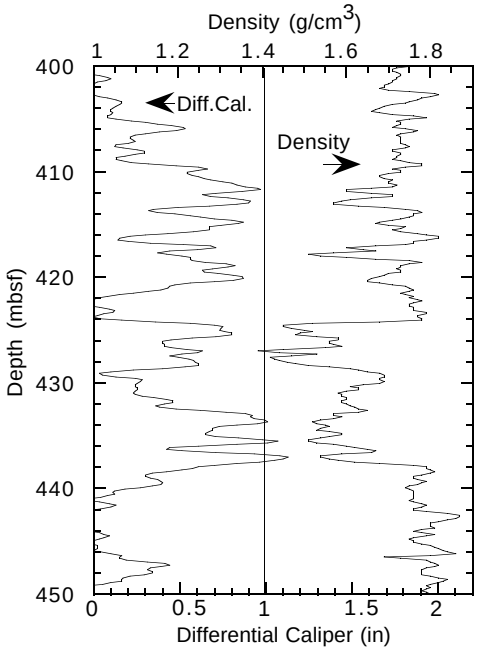

Figure 9. Comparison of the density and differential caliper logs between 400 and 450 mbsf at Site 1044.

g/cm^3, similar to the low densities observed in the proto-décollement zone at Site 1044. Unit 7 from Site 1045 is thinner than the proto-décollement zone at Site 1044; therefore, the former is interpreted as a zone of residual underconsolidation.

Below the décollement zone at Site 1045, densities increase sharply, whereas the density increase below the Site 1044 proto-décollement zone occurs more gradually. The density offset between Sites 1044 and 1045 decreases with depth below the décollement zone, and the curves converge near the bottom of the Hole 1045A density log. The small density difference between the two sites indicates that little compaction has occurred within this underthrust section. Limited compaction is also suggested by the reasonable correlation between the features of the two logs. The resistivity logs from the underthrust section of the two boreholes are similar in character. However, the Site 1045 resistivities are consistently lower than those at Site 1044. This relationship is surprising because, in general, resistivity increases as bulk density increases.

Summary

1. The density log shows several clear-cut divisions that can be correlated with first-order structural discontinuities. Prominent faults are inferred at about 45, 165, and 318 mbsf from offsets and reversals in downhole trends; those at 45 and 318 mbsf can be matched to faults in the seismic section.
2. The décollement zone is clearly identified in both the density log and the resistivity log by offsets toward lower absolute values.
3. The top of the underthrust sequence shows remarkably little evidence of consolidation in comparison with the reference section at Site 1044.

LOGS AND INDICATORS OF FLUID FLOW

Shipley et al. (1994) proposed that negative polarity seismic reflections along the décollement zone are caused by dilation resulting from high fluid pressures. One goal of drilling Site 1045 was to test this hypothesis. In addition, anomalous values in chemical and thermal data collected during Leg 110 were used to infer fluid migration along the décollement zone and major thrusts in the accretionary prism. In this section, we discuss whether the LWD data indicate the presence of elevated fluid pressures and fluid migration along major thrusts and the décollement zone. The relevant LWD data are presented in Figure 7 (see "Logs and Structure" section, this chapter), along with the locations of major thrust faults interpreted from the seismic data and other thrusts postulated from the log data.

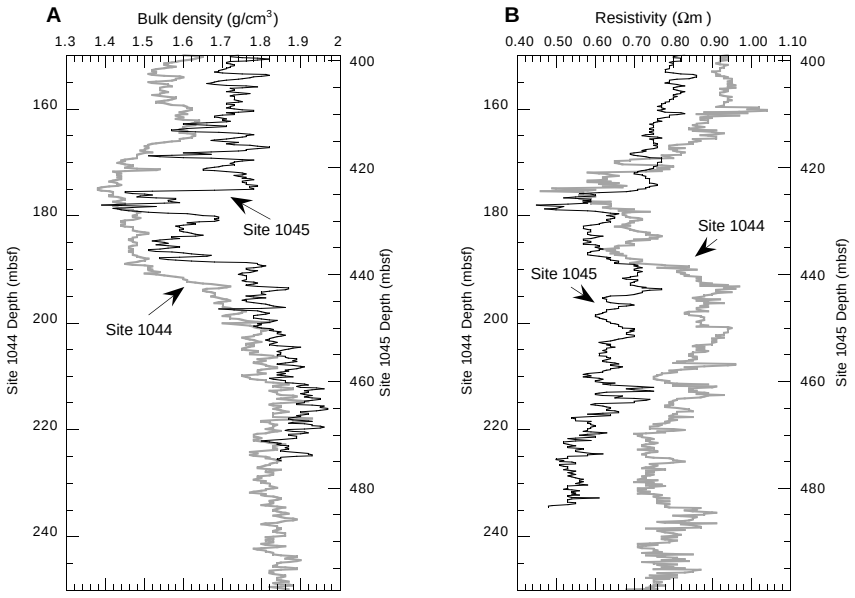

Figure 10. **A.** Comparison of the density profiles in and below the proto-décollement zone at Site 1044 and below the décollement zone at Site 1045. **B.** Comparison of the deep resistivity profiles in and below the proto-décollement zone at Site 1044 and below the décollement zone at Site 1045.

Log Unit 6

Within log Unit 6, the density, photoelectric effect, gamma-ray, and resistivity logs decrease to the top of the décollement zone at 425 mbsf. These decreases cannot be attributed to any plausible lithology change (see "Logs and Lithology" section, this chapter). They are more consistent with an increase in porosity. A major thrust was identified in the seismic reflection profile at 334 mbsf (see "Logs and Structure" section, this chapter), near the top of log Unit 6. The downward monotonic decrease in density between this thrust and the décollement zone is best explained by a pressure source along the décollement zone, with drainage along the overlying thrust fault.

Décollement Zone (Log Unit 7)

Within the décollement zone (log Unit 7), the density, photoelectric factor, and resistivity logs show local minima. The low values in the lithologic indicator logs appear to be caused by the low densities of the sediments in this unit. There are two possible reasons for the low densities. The sediments may be underconsolidated because of the low permeabilities of the overlying wedge. Alternatively, the sediments may be dilated by injection of high fluid pressures from arcward in the wedge (Brown et al., 1994; Shipley et al., 1994). It was possible to make a preliminary assessment of whether the low densities are caused by dilation of the fault or by underconsolidation. The lowest density value in the center of the décollement zone is 1.4 g/cm^3. On the basis of previous drilling results and seismic data (Shipboard Scientific Party, 1988a), this unit correlates lithologically with the proto-décollement zone (log Unit 2) at reference Site 1044. Within this unit, the density also reaches a local minimum of 1.4 g/cm^3. Although the density log signatures are not identical (see "Logs and Physical Properties" section, this chapter; Fig. 10), the equivalent minimum density values suggest roughly equivalent effective stress states in the two locations. Thus, the low-density intervals of log Unit 7 may have experienced almost no consolidation during the time it took these sediments to reach this location. Consequently, dilation by injection of fluids, although still a possibility, is not required to explain the LWD data from the décollement zone.

Other Thrust Faults

On the basis of geochemical and thermal data from Leg 110, it is apparent that major thrust faults in the prism can carry significant fluid flow from depth (Gieskes et al., 1990; Fisher and Hounslow,

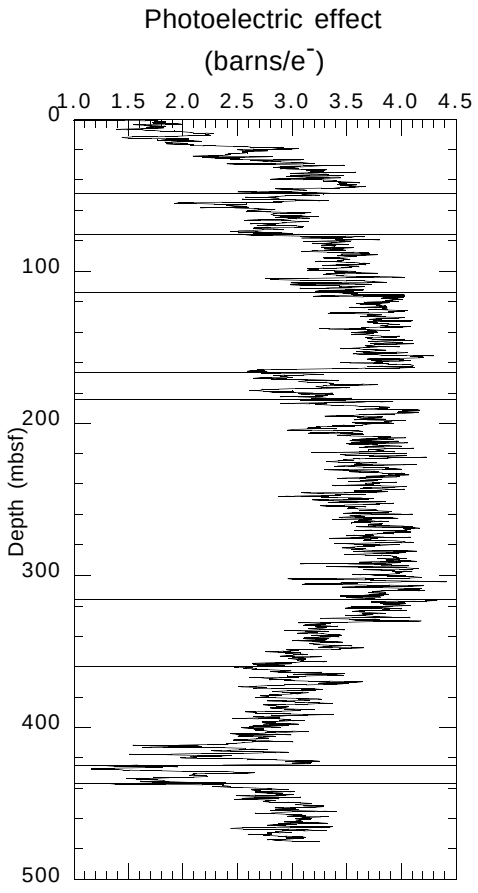

Figure 11. Photoelectric effect vs. depth in Hole 1044A. Lines separate intervals discussed in the text (major and minor log units).

1990). At Site 1045, there are several indications in the LWD data of possible elevated fluid pressures along thrust faults. The caliper log data are shown in Figure 7. Peaks in the caliper log indicate intervals where conditions may have caused the hole to widen. The four peaks in the differential caliper data are at 40–80, 170, 250, and 400–440 mbsf. Recorded pressures and pumping rates were uniform during

drilling below 140 mbsf, indicating that the lower three peaks are not related to variations in drilling procedure. Therefore, these high caliper readings could be caused either by a significant lithology change or by an increase in formation pressure. The sediments in the prism consist of marls, muds, and clays, with thin ash units (Shipboard Scientific Party, 1988a). Based on the uniform mechanical properties of these sediments, it seems likely that the second and third peaks in the caliper log are caused by changes in the formation pressure. These peaks in the caliper log do not correlate with faults that are clearly imaged in the seismic data. However, they do correlate with decreases in the density, photoelectric effect, and resistivity logs, suggesting that the caliper data are a potential indicator of fluid-flow zones. The peak in the caliper data at 400–440 mbsf correlates with the décollement zone and the inferred underconsolidated area just above it.

Summary

1. The décollement zone and the overlying section have low densities that can be attributed to underconsolidation. Although dilation is possible, it is not necessary to explain the low densities.
2. High values in the differential caliper log correlate with the décollement zone. Two other locations with high values correlate with changes in other logs and thus may also indicate zones of elevated fluid pressure.
3. The LWD data from all Leg 171A sites must be further analyzed to determine if the caliper log is a reliable indicator of fluid flow.

LOGS AND SEISMIC DATA

Synthetic Seismogram

The synthetic seismogram for Site 1045 was constructed using an assumed velocity profile, as described in the "Explanatory Notes" chapter (this volume). At Site 1045 the velocity profile consists of a linear gradient from 1.5 km/s at the seafloor to 1.85 km/s at the bottom of the hole. This is the same gradient that was used at Site 1044.

The synthetic seismogram shows a reasonably good match to the décollement-zone reflection observed in the 3-D seismic data at this site (Fig. 13). The décollement zone corresponds to a 14-m-thick interval of low density (1.4–1.6 g/cm^3) between 424 and 438 mbsf in the log data. The waveforms of the décollement zone correlate well between the synthetic and real data, indicating a good match between the low-density interval and the position of the seismically defined décollement zone. The sharp boundaries at the top and base of this low-density interval produce reflections of opposite polarity, which constructively interfere to produce a strong décollement-zone reflection at this site. One of the main discrepancies between the décollement-zone reflection in the synthetic seismogram and the data is that the lower positive lobe of the décollement zone (filled area) is noticeably larger in amplitude in the synthetic trace than in the seismic data. This difference is possibly due to changes in velocity, data that we lack for calculation of the synthetic trace.

Other low-density intervals observed in the log produce distinct reflections in the synthetic trace. The shallowest low-density interval is at 50 mbsf, and it produces a strong reflection in the synthetic trace at this depth. This low-density interval may correlate with one of two faults that appear to surface at a break in the seafloor 60 m east of Site 1045. The reflection of the fault plane in the data has significantly weaker amplitude than that observed in the synthetic trace. A low-density interval between 160 and 185 mbsf also produces a noticeable reflection in the synthetic trace, with no correlative reflection of equivalent amplitude in the seismic data. The few reflections that are observed at this depth are continuous over no more than two to three traces (30–45 m), and this low-density interval does not correlate well with any distinct fault in the seismic section. A possible explanation for the mismatch between the amplitudes of the reflections observed in the data and in the synthetic trace is that these low-density intervals are steeply dipping (>30°) and are not well imaged in the 3-D seismic data.

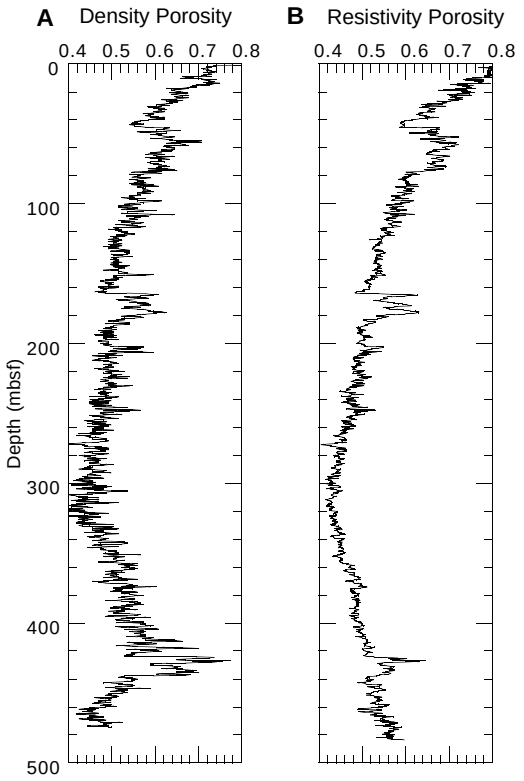

Figure 12. Calculated Site 1045 (**A**) density porosity and (**B**) resistivity porosity vs. depth.

REFERENCES

Bangs, N.L.B., Shipley, T.H., and Moore, G.F., 1996. Elevated fluid pressures and fault zone dilation inferred from seismic models of the northern Barbados Ridge décollement. *J. Geophys. Res.*, 101:627–642.

Bekins, B.A., McCaffrey, A.M., and Driess, S.J., 1995. Episodic and constant flow models for the origin of low-chloride waters in a modern accretionary complex. *Water Resour. Res.*, 31:3205–3215.

Brown, K.M., Bekins, B., Clennell, B., Dewhurst, D., and Westbrook, G., 1994. Heterogeneous hydrofracture development and accretionary fault dynamics. *Geology*, 22:259–262.

Fisher, A.T., and Hounslow, M.W., 1990. Heat flow through the toe of the Barbados accretionary complex. *In* Moore, J.C., Mascle, A., et al., *Proc. ODP, Sci. Results*, 110: College Station, TX (Ocean Drilling Program), 345–363.

Gieskes, J.M., Vrolijk, P., and Blanc, G., 1990. Hydrogeochemistry, ODP Leg 110: an overview. *In* Moore, J.C., Mascle, A., et al., *Proc. ODP, Sci. Results*, 110: College Station, TX (Ocean Drilling Program), 395–408.

Moore, G.F., Zhao, Z., Shipley, T.H., Bangs, N., and Moore, J.C., 1995. Structural setting of the Leg 156 area, northern Barbados Ridge accretionary prism. *In* Shipley, T.H., Ogawa, Y., Blum, P., et al., *Proc. ODP, Init. Repts.*, 156: College Station, TX (Ocean Drilling Program), 13–27.

Screaton, E.J., Wuthrich, D.R., and Dreiss, S.J., 1990. Permeabilities, fluid pressures, and flow rates in the Barbados Ridge Complex. *J. Geophys. Res.*, 95:8997–9007.

Shipboard Scientific Party, 1988a. Site 671. *In* Mascle, A., Moore, J.C., et al., *Proc. ODP, Init. Repts.*, 110: College Station, TX (Ocean Drilling Program), 67–204.

————, 1988b. Site 672. *In* Mascle, A., Moore, J.C., et al., *Proc. ODP, Init. Repts.*, 110: College Station, TX (Ocean Drilling Program), 205–310.

————, 1995a. Site 947. *In* Shipley, T.H., Ogawa, Y., Blum, P., et al., *Proc. ODP, Init. Repts.*, 156: College Station, TX (Ocean Drilling Program), 71–86.

————, 1995b. Site 949. *In* Shipley, T.H., Ogawa, Y., Blum, P., et al., *Proc. ODP, Init. Repts.*, 156: College Station, TX (Ocean Drilling Program), 193–257.

Shipley, T.H., Moore, G.F., Bangs, N.L., Moore, J.C., and Stoffa, P.L., 1994. Seismically inferred dilatancy distribution, northern Barbados Ridge décollement: implications for fluid migration and fault strength. *Geology*, 22:411–414.

Tobin, H.T., and Moore, J.C., 1997. Variations in ultrasonic velocity and density with pore pressure in the décollement zone, northern Barbados Ridge accretionary prism. *In* Shipley, T.H., Ogawa, Y., Blum, P., Bahr, J.M. (Eds.), *Proc. ODP, Sci. Results*, 156: College Station, TX (Ocean Drilling Program), 125–136.

Tribble, J.S., 1990. Clay diagenesis in the Barbados accretionary complex: potential impact on hydrology and subduction dynamics. *In* Moore, J.C., Mascle, A., et al., *Proc. ODP, Sci. Results*, 110: College Station, TX (Ocean Drilling Program), 97–110.

Underwood, M.B., and Deng, D., 1997. Clay mineralogy and clay geochemistry in the vicinity of the décollement zone, northern Barbados Ridge. *In* Shipley, T.H., Ogawa, Y., Blum, P., and Bahr, J.M. (Eds.), *Proc. ODP, Sci. Results*, 156: College Station, TX (Ocean Drilling Program), 1–32.

Wang, Y.-C., Gieskes, J.M., and Musoke, L., 1990. Bulk chemical analysis of sediments—Hole 671B. *In* Moore, J.C., Mascle, A., et al., *Proc. ODP, Sci. Results*, 110: College Station, TX (Ocean Drilling Program), 179–188.

Ms 171AIR-104

NOTE: For all sites drilled, shore-based log processing data are available on CD-ROM. See Table of Contents for material contained on CD-ROM.

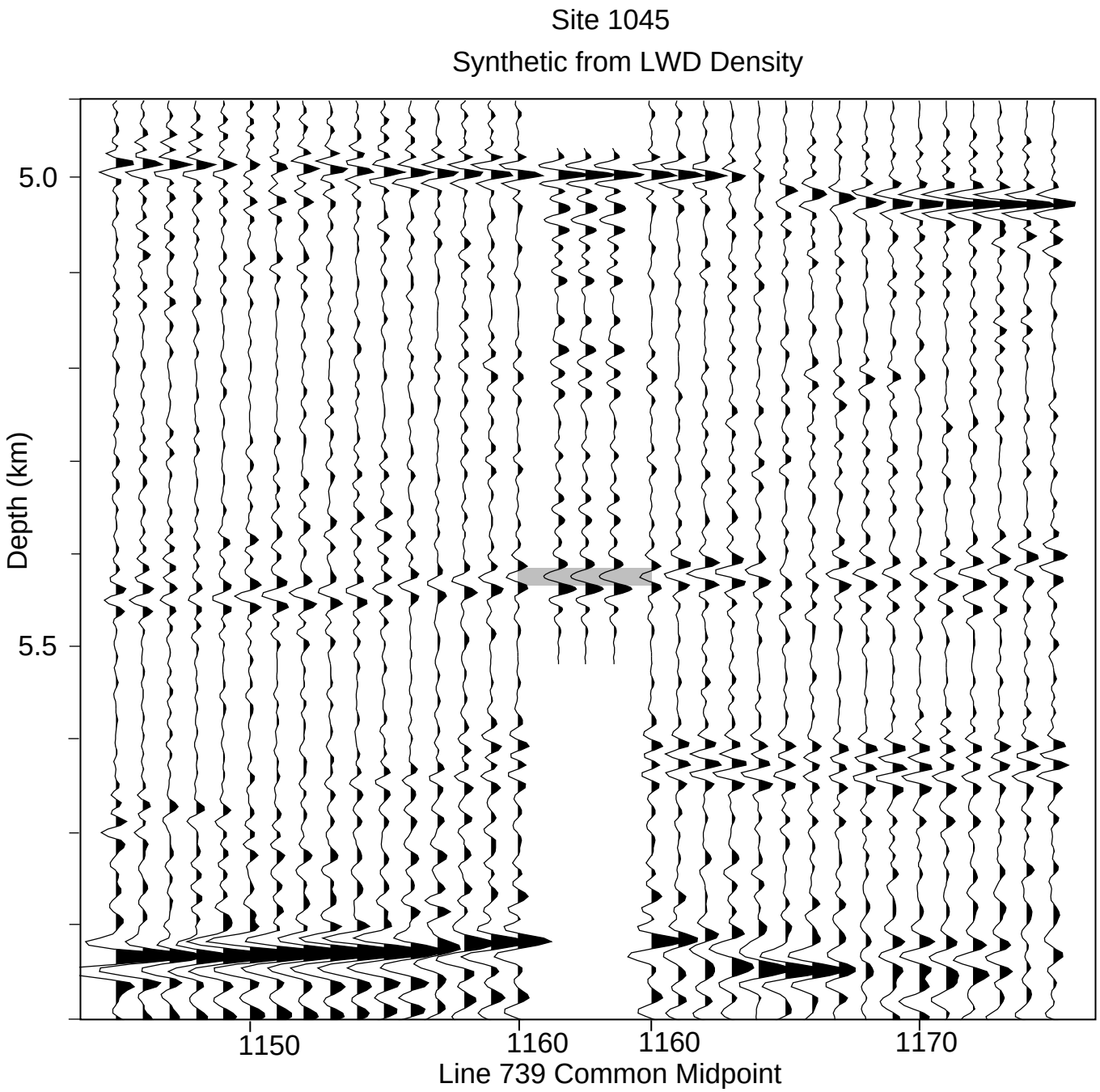

Figure 13. Three identical synthetic traces are shown at Site 1045 on Line 739. The shaded area shows the location of the décollement zone, as indicated by the density log. See “Explanatory Notes” chapter (this volume) for a description of the synthetic seismogram construction. Trace spacing is 15 m; vertical exaggeration is 0.5×.

Prior Chapter Contents Next Chapter